Heterogeneous & Homogeneous & Bio- & Nano-
CHEMCATCHEM
CATALYSIS

Accepted Article

Title: Synthetic & Catalytic Potential of Amorphous Mesoporous Aluminosilicates Prepared by Post-Synthetic Aluminations of Silica in Aqueous Media

Authors: Roel Locus, Danny Verboekend, Martin d'Halluin, Michiel Dusselier, Yuhe Liao, Nicolas Nuttens, Tony Jaumann, Steffen Oswald, Luis Mafra, Lars Giebeler, and Bert Sels

This manuscript has been accepted after peer review and appears as an Accepted Article online prior to editing, proofing, and formal publication of the final Version of Record (VoR). This work is currently citable by using the Digital Object Identifier (DOI) given below. The VoR will be published online in Early View as soon as possible and may be different to this Accepted Article as a result of editing. Readers should obtain the VoR from the journal website shown below when it is published to ensure accuracy of information. The authors are responsible for the content of this Accepted Article.

To be cited as: *ChemCatChem* 10.1002/cctc.201701660

Link to VoR: http://dx.doi.org/10.1002/cctc.201701660

A Journal of
ChemPubSoc Europe

WILEY-VCH

www.chemcatchem.org

WILEY-VCH

DOI: 10.1002/ ((please add manuscript number))
Article type: Full Paper

Synthetic & Catalytic Potential of Amorphous Mesoporous Aluminosilicates Prepared by Post-Synthetic Aluminations of Silica in Aqueous Media

Roel Locus, Danny Verboekend, Martin d'Halluin, Michiel Dusselier, Yuhe Liao, Nicolas Nuttens, Tony Jaumann, Steffen Oswald, Luís Mafra, Lars Giebeler, Bert Sels**

Dr. R. Locus, Dr. D. Verboekend, Dr. M. d'Halluin, Dr. M. Dusselier, Y. Liao, N. Nuttens, Prof. B. F. Sels
Center for Surface Chemistry and Catalysis, KU Leuven,
Celestijnenlaan 200F, Bus 2461, B-3001 Heverlee, Belgium
E-mail: danny.verboekend@kuleuven.be, bert.sels@kuleuven.be

Dr. T. Jaumann, Dr. S. Oswald, Dr. L. Giebeler
Leibniz-Institute for Solid State and Materials Research (IFW) Dresden e.V., Institute for Complex Materials, Helmholtzstr. 20, D-01069 Dresden, Germany

Dr. L. Mafra
CICECO - Aveiro Institute of Materials, Department of Chemistry, University of Aveiro, Campus Universitário de Santiago, 3810-193 Aveiro, Portugal

Keywords: amorphous aluminosilicates, silica, alumination, acidity, catalysis

Accepted Manuscript

This article is protected by copyright. All rights reserved.

Abstract

Amorphous aluminosilicates catalysts have been used industrially on a large scale for almost a century. However, the influence of the pH on the alumination of silica in aqueous solutions has remained largely unclear. Herein, room temperature aluminations of different mesoporous amorphous silicas (fumed silica, dried silica gel, SBA-15, MCM-41, and COK-12) with aqueous solutions of various pH (3-13) are explored. The aqueous solutions are prepared using different aluminum sources ($Al(NO_3)_3$ or $NaAlO_2$) and alkaline additives (NaOH or NH_4OH). The decoupling of pH and Al source using alkaline additives results in a vast experimental potential to prepare unique aluminosilicates, where an important role is played by the pH development during the treatment. The bulk and surface composition, acidity, aluminum coordination, morphology, hydrothermal stability, and porosity of the obtained materials are characterized. Optimal samples possess large surface areas and superior acidities (up to 50% higher) and outstanding stabilities compared to aluminosilicates prepared *via* state of the art methods. The obtained materials are evaluated in a series of acid-catalyzed model reactions involving substrates of various chemical reactivity and size, enabling insight in the catalytic functionality of the introduced Brønsted and Lewis sites. The potential of the obtained materials is emphasized by the similar or superior acidity and catalytic performance compared to several benchmark industrial silica-alumina-based catalysts.

Accepted Manuscript

This article is protected by copyright. All rights reserved.

1. Introduction

Porous amorphous aluminosilicates are amongst the most important heterogeneous acid catalysts because of their active acid sites, a facile recoverability, high regeneration ability, and a relatively easy synthesis.[1] Combined with the large abundance of silicon and aluminum, these properties render them environmentally-friendly and industrially-viable catalyst.[1,2] Mesoporous amorphous silica-alumina (ASA) are accordingly used on large scale in the hydrocracking of heavy oil fractions to middle distillates, as active matrix for pre-cracking of heavy hydrocarbon fractions in fluidized catalytic cracking particles, in the dehydrochlorination of chlorinated hydrocarbons, and numerous others.[2-5]

The advantage of ASA over (purely Lewis acidic) alumina is that Brønsted acid sites are formed when monomeric aluminum is incorporated in the silica framework with a tetrahedral coordination (isomorphous substitution).[6,7] Still, the exact nature of the acidity of ASAs can be rather complex due to their large heterogeneity.[8-16] Not only the relative quantity of silica and alumina can strongly vary, but also their distribution (zoning, gradients, etc.), their coordination (in the case of Al: tetrahedral/framework *versus* octahedral/extra-framework), and accessibility (isolated aluminum atoms within the bulk or accessible on the surface). Based on these issues, the total acidity of the ASA is usually much lower (generally <100 μmol g^{-1}, **Table S1**), compared to the total aluminum content in the aluminosilicate catalysts.

ASAs can be synthesized using a variety of bottom-up and top-down methods, such as co-precipitation, grafting, and deposition, all of which involve the contacting of a silica source with an aluminum source or *vice versa*.[8-16] One of the most used (and commercially attractive) methods may be the deposition of Al by subjecting silica to Al-containing aqueous solutions, taking advantage of the hydrolysis-condensation behavior of Al^{3+} ions in water. The latter is typically performed using various Al salts such as $Al_2(SO_4)_3$, $Al(NO_3)_3$, and $NaAlO_2$. Unlike the aforementioned salts, $NaAlO_2$ forms an alkaline solution after dissolution, and has yielded materials with relatively high acidity.[14,16,17] This observation implies that control of

This article is protected by copyright. All rights reserved.

Accepted Manuscript

the pH may be beneficial for the creation of acid sites. However, despite an early indication of this beneficiary effect,[18,19] the influence of the pH on the alumination of silica in aqueous solutions has never been subjected to a dedicated study.

Herein, we present the post-synthetic alumination of silica using aqueous solutions of varying pH as a facile technique to prepare aluminosilicate catalysts featuring superior physico-chemicals properties and outstanding catalytic performance compared to conventional silica-aluminas. In a case study on the widely-studied model system SBA-15, the effects of the alumination step on the porous, compositional, structural, and acidic properties are disclosed. Within the compositional range studied, high solid yields are combined with total acidities that exceed the maximum values reported in the literature by *ca.* 50%. In addition, the overall porosity is largely preserved and the hydrothermal stability is enhanced. The aluminated SBA-15 samples showed exceptional activities and selectivities in various Lewis and Brønsted acid-catalyzed model reactions, such as alkylation, isomerization, and cracking. Furthermore, the versatility of the method is emphasized by the successful extrapolation towards various ordered (MCM-41 and COK-12) and non-ordered silica sources, such as fumed silica and dried silica gel.

Accepted Manuscript

This article is protected by copyright. All rights reserved.

2. Results and Discussion

The pH development prior to and during the alumination of silicas in aqueous media is discussed in **Section 2.1**. Next, in **Section 2.2**, the synthesis and characterization of the aluminated SBA-15 materials is discussed. SBA-15 was selected as a model type for amorphous mesoporous silica because of the well-defined 1D ordered pore system. In **Section 2.3** an extrapolation to other ordered and non-ordered amorphous silicas is presented. Next, in **Section 2.4** selected samples are catalytically evaluated and compared to several commercial amorphous and crystalline aluminosilicates standards. Finally, the relationships between the active solid catalyst, pH, acidity, and activity are discussed (**Section 2.5**).

2.1. The Role of pH during the Alumination of Silica in Aqueous Media

The pH in the used aqueous solutions depends on the nature and quantity of the type of Al salt and the base (**Figure 1a**). For example, the addition of $Al(NO_3)_3$ to distilled water causes a drop in pH to a plateau value of ~3, due to complexation of the OH^- ions by Al^{3+} ions. To create alumination solutions with higher pH three other types of solutions were employed. First, solutions of $NaAlO_2$ were studied ('0-*x*-$NaAlO_2$' samples, where '*x*' refers to the applied Al concentration [$Al_{initial}$]). These solutions display an increasing pH as a function of $[Al]_{initial}$ due to the increased release of OH^- ions. Nevertheless, as with $Al(NO_3)_3$, the alkalinity in these solutions remains directly connected to the amount of Al. Conversely, by complementing the Al source ($Al(NO_3)_3$) with a certain amount of base, the pH and the Al concentration are decoupled. NaOH and NH_4OH were selected as references for strong and weak bases, respectively. NaOH completely dissociates in water, whereas NH_4OH yields a partial dissociation ($K_b = 1.8 \cdot 10^{-5}$) and has a buffering effect on the pH.[22] For the sake of conciseness, we have fixed the base concentrations of NaOH (0.1 M) and NH_4OH (0.5 M) within this contribution. These base concentrations were selected based on the recent work on the enhancement of the acidity of Al-containing MCM-41 by base treatments.[20] In the case

This article is protected by copyright. All rights reserved.

Accepted Manuscript

of the solutions with NaOH ('0-*x*-NaOH' samples) the pH reduces due to the complexation of hydroxyls to form the aluminate ions ($Al(OH)_4^-$). For aluminations with NH_4OH on the other hand, a buffering effect is observed in the form of a plateau at a pH of ~ 10 for increasing aluminum concentrations ('0-*x*-NH_4OH' samples). The measured pH curves in **Figure 1a** agree well with the calculated ones (**Figure S1**). It should be noted that a solid alumina phase can form in Al-containing solutions when the pH is reduced to ~10 and lower.[21] The formation of alumina (and its hydroxides) occurred in samples 0-0.03-NaOH, 0-0.02-NH_4OH and 0-0.03-NH_4OH, and was observed as a transformation in the solution from clear to colloidal white (**Figure S2**). Accordingly, aluminations of silicas were systematically performed by mixing the silica and the Al source directly with the base, rather than first mixing the Al source with the base, followed by the addition of the silica.

During the aluminations of silica SBA-15, the pH decreases as a function of time (**Figure 1b-c**). This change is explained partially by the low isoelectric point of silica (about 2-3), combined with the consumption of hydroxyl ions by the gradual dissolution of silica.[23] The latter is proven by the pH-time profile of S-0-NaOH, in which the absence of Al implies that the reduction of the pH is largely due to the consumption of hydroxyl ions by the silica dissolution. When aluminum is present, the pH lowering is more pronounced. For S-0.03-NaOH the pH dropped to almost neutral (pH ~ 6) and for S-0.04-NaOH (not shown) even to 3.7. For the alumination with NH_4OH, the buffering effect on the pH is obvious (**Figure 1c**). Only a small initial change of pH is observed after the addition of the Al and the silica (0-2 min) to the ammonium hydroxide solution, and the pH remained constant (around 10.5) during the remainder of the treatment. During aluminations with $NaAlO_2$, the pH increased to above 10 within the first minute after the addition of distilled water to the mixture of silica and $NaAlO_2$. Afterwards this initial increase the pH reduced gradually, reaching approximately 9 after 30 min.

This article is protected by copyright. All rights reserved.

Accepted Manuscript

2.2. Synthesis and characterization of aluminated ordered mesoporous silica

The different alumination techniques and the properties of the parental and the resulting materials are summarized in **Table 1**. A first important criterion after any post-synthetic modification is the mass yield (Y), which is particularly relevant in this case as silica readily dissolve in alkaline solutions (pH > 10). Mass yields of S-*x*-NaOH and S-*x*-NH_4OH for aluminum concentrations ($[Al]_{initial}$) lower than 0.006 M are around 75%, but for higher $[Al]_{initial}$ mass yields nearly reach 100% indicating a negligible loss of silica (**Figure 2a**). The increasing yields likely relate to the lower pH at increasing $[Al]_{initial}$. Still, the increased solid yield may also be due the increased resistance of the solid to alkaline leaching as the covering of silica by Al surface species.[24] For example, even though the pH of solutions with $NaAlO_2$ increases with Al content, aluminations with $NaAlO_2$ did not show a reduced mass yield as a function $[Al]_{initial}$. The absence of such trend confirms that, besides the pH, also other factors such as the Al content have a pronounced influence on the dissolution of silica.

Bulk (Si_{ICP}/Al_{ICP}) and surface (Si_{XPS}/Al_{XPS}) composition evidenced the absence of Al in the parent SBA-15 (S-P, **Table 1** and **Figure 2b**). An Al incorporation of ~90% into the samples S-*x*-NaOH and ~85% in S-*x*-NH_4OH was achieved (**Figure 2b,c**). On the other hand, alumination with $NaAlO_2$-based solutions led to an incorporation of less than 60% of the initial Al into the respective silica. The Si/Al ratios are lower for the surface(-near) species compared to the bulk, suggesting that most Al is incorporated near the surface of the pores and/or the outer surface of the particles. This result follows logically from post-synthesis alumination by a solution, differing to aluminations during silica synthesis (as for example in Al-MCM-41). In the latter case, the surface Si/Al ratios are often higher than the bulk ratios because of the incorporation of Al into the pore walls rather than on the surface.[20]

The porous properties of the samples before and after aluminations were analyzed with N_2 physisorption (**Figures 3a,b** and **S3**). The typical type IV nitrogen isotherms with type A hysteresis loops were observed, indicating capillary condensation in (cylindrical) mesopores

This article is protected by copyright. All rights reserved.

Accepted Manuscript

in the parent SBA-15.[25] A sharp pore size distribution (PSD) of ~7 nm was combined with a high specific surface area > 500 m^2 g^{-1} and high pore volumes > 0.5 cm^3 g^{-1}. For S-*x*-NaOH samples, the average pore size (d_p) did not change after alumination, but the PSDs became broader, forming pores up to 20 nm for $[Al]_{initial}$ lower than 0.015 M. The amount of micropores decreased after this type of alumination on SBA-15, as is indicated by the lower N_2 uptake at p/p_0<0.2. These trends are explained by Ostwald ripening, which is catalyzed by OH^- ions. Pores with larger sizes expanded at the expense of smaller pores, which were filled up with a portion of the etched silica from the larger pores.[20,21] The isotherms and pore size distributions of S-*x*-NH_4OH and S-*x*-$NaAlO_2$ samples remained mostly the same upon treatment (**Figure S3**). As for the S-*x*-NaOH samples, the largest changes in pore size occurred in aluminations with the highest pH (and thus the lowest $[Al]_{initial}$). The evolution in the PSDs after different aluminations was in good resemblance with the trends obtained on mildly alkaline-treated Al-MCM-41.[20]

The pore volume (V_{pore}) and specific surface area (S_{BET}) showed comparable trends after aluminations (**Table 1**). Generally, V_{pore} and S_{BET} decreased by *ca.* 20% in alkaline media. This behavior is partially explained by the filling of smaller micro- and mesopores by Ostwald ripening and the deposition of Al(-oxide) species in these smaller pores. For the S-*x*-NaOH samples an increasing Al content reduced the negative influence on V_{pore} and S_{BET} by an increased neutralization of the solution. This neutralization did not occur for the S-*x*-NH_4OH and S-*x*-$NaAlO_2$ samples. In the former, the buffering effect caused an almost constant pH and in the latter the pH increased with the aluminum concentration. In general, the changes in porosity related well with the yield. Moreover, a general observation is that as long as the yield exceeded 90%, a limited effect on the porosity is achieved.

The 1D-hexagonal pore ordering in SBA-15 enables a straightforward analysis of the effect of the aluminations on the porous structure using transmission electron microscopy (TEM). In the parent material the ordered mesopores were clearly visible (**Figure 4**). After aluminations

This article is protected by copyright. All rights reserved.

Accepted Manuscript

in NaOH with $[Al]_{initial}$ of 0.002 M and 0.015 M domains significantly appeared less ordered, especially near the edges of the particles. This observation suggests that the highest reactivity of the hydroxyls occurs at the outside of the silica particles. The latter may relate to the existence of accessibility limitations, inhibiting the hydroxyls to reach bulk regions in the unidirectional SBA-15 pores. In the sample S-0.03-NaOH no pore transformation was observed, in agreement with the observed high mass yields and preserved porosities. No significant effect on the particle size was detected by TEM.

Alumination of amorphous silica samples can induce two major types of Al coordination. Tetrahedral Al (Al^{IV}) relates to Al species fully incorporated into the silica network, whereas octahedral Al (Al^{VI}) indicates the presence of extra-structure Al_2O_3 domains.[6] In the treated samples, at least two types of Al coordination can be distinguished using ^{27}Al MAS NMR: Al^{IV} sites resonating at ~54 ppm, while Al^{VI} sites resonate at ~0 ppm.[6] The NMR spectrum of S-0.03-NaOH reveals around 70% tetrahedral aluminum, which is similar to the commercial benchmark aluminosilicate (ASA-6, **Figure S4**).

To monitor the introduced acidity, pyridine-probed Fourier transformed infra-red spectroscopy (PP-FTIR) experiments were conducted (**Table 2** and **Figure 5**). In the S-*x*-$NaAlO_2$ samples a plateau value was achieved both in Brønsted (B) and in Lewis (L) acidity (~30 and ~70 µmol g^{-1}, respectively) for $[Al]_{initial} \geq 0.015$ M. For the S-*x*-NaOH samples on the other hand, B and L acidity were lower compared to the SBA-15 treated with the solution of $NaAlO_2$ for $[Al]_{initial} < 0.03$ M. However, a higher acidity was reached for S-0.03-NaOH (B = 60 µmol g^{-1} and L = 78 µmol g^{-1}). With higher concentrations of aluminum (S-0.04-NaOH) the acidity was substantially lower (B = 31 µmol g^{-1}, L = 76 µmol g^{-1}). Compared to the S-*x*-NaOH samples, the increase in acidity with increasing $[Al]_{initial}$ was lower for the S-*x*-NH_4OH samples (B = 39 µmol g^{-1} and L = 78 µmol g^{-1}, for S-0.03-NH_4OH). However, the latter acidity of S-0.03-NH_4OH was higher compared to S-0.03-$NaAlO_2$. In general, the ratio of B/L was roughly constant at 0.4 for the $NaAlO_2$-treated samples. The NH_4OH and NaOH-treated

This article is protected by copyright. All rights reserved.

Accepted Manuscript

samples yielded B/L ratios of ≥0.5, which were less constant over the Al concentration applied. Both bases yielded a relatively high B/L ratio (about 0.7) at 0.006 M, which reduced to 0.5 at higher concentrations ($[Al_{initial}]$>0.006 M). Exceptionally, S-0.03-NaOH yielded a B/L of nearly 0.8, which is tentatively attributed to the significant pH change during the treatment (**Figure 1c**, *vide supra*). The Brønsted and the total acidity in S-0.03-NaOH are amongst the highest values achieved for amorphous silica-alumina both commercial and in literature (**Figure 6a,b**). Moreover, for Si/Al ratios exceeding 15, sample S-0.03-NaOH features over 50% higher Bronsted and 30% higher total acidity compared to the state of the art. The latter is a significant result, particularly taking into account the affordable nature of the reagents, and the ease of the procedure, and the vast potential to further optimize the alumination protocol.

A measure to assess the accessibility of the aluminum atoms introduced into the silica is to normalize the number of formed acid sites (B + L) by the total amount of aluminum (Al_{ICP}). This measure, also referred to as the effective acidity (EA), was recently used to highlight acidity changes upon pH-controlled activation of Al-containing MCM-41.[20] At $[Al]_{initial} \leq 0.02$ M, the EA values are highest for S-*x*-$NaAlO_2$ samples followed by samples obtained by treatment in NH_4OH and NaOH, respectively (**Figure 5d**). Nevertheless, at increasing $[Al]_{initial}$ the effective acidities converge to around 20% (at 0.03 M), with S-0.03-NaOH displaying the highest EA. This lowering of the EA as a function of $[Al]_{initial}$ is attributed to the decreased number of isolated acidic Al located on the external surface, which relates well with the increased Si_{XPS}/Al_{XPS} ratios (**Figure 2c**). Such trend accords with the existing literature, where the highest reported EA values follow a quasi-linear increase from about 5% at Si/Al = 10 to about 30% at Si/Al = 60 (**Figure 6c**). Within these references, the effective acidity of the samples prepared by the alumination display among the highest, showing that the described techniques yield rather accessible Al sites. In addition, sample 'M50-0-NaOH', derived from ref. [20] and prepared by optimized mild alkaline treatment of

This article is protected by copyright. All rights reserved.

Accepted Manuscript

Al-containing MCM-41, confirms that preparing aluminosilicates at the appropriate pH yields the highest effective acidities.

The hydrothermal stability of aluminosilicates is an important parameter in many catalytic applications. Stability tests in boiling water form a suitable test to assess hydrothermal stability,[27] and were executed on selected samples. After the treatment, the porosity of the samples was measured (**Table 1**). The parent silica (S-P) showed a pronounced one-third reduction in BET surface area. Conversely, the aluminated samples treated with $[Al]_{initial}$ of 0.015 to 0.03 M (Si/Al ratios of ca. 20-50) featured similar or even slightly enhanced BET surface areas (increase up to 10%). Moreover, the aluminated samples displayed a substantially higher stability in boiling water compared to a commercial aluminosilicate (ASA-6), which showed a 16% decrease in BET surface area.

An increase of the stability of the aluminated materials compared to the parental silicas may be expected based on the higher Al content.[27] However, the Al content alone cannot explain the superior stability of the aluminated samples compared to the commercial reference ASA-6. In this case, the superior stability can be attributed to the more selective deposition of Al on the external surface. As mentioned above, in ASA-6 more aluminum is likely localized in the bulk as typical for silica syntheses with both Al and Si precursors, where it is unable to protect the silica framework in many cases.[27] As the effective acidity is directly linked to the Al distribution, the stability test results can be related to the effective acidity. Hence, the effective acidity can act as an indirect indicator of the hydrothermal stability of amorphous aluminosilicates. Naturally, more dedicated study is required to verify the latter hypothesis. Nevertheless, the potential relationship implies that even when the porosity and acidity of the aluminosilicates prepared by post-synthetic alumination are similar to that of a commercial sample, the use of the post-synthetic technology remains advantageous as the solids are more likely to maintain their physico-chemical properties in the catalytic cycle.

This article is protected by copyright. All rights reserved.

Accepted Manuscript

2.3. Extrapolation to Ordered and Non-Ordered Amorphous Silica

Other ordered and non-ordered mesoporous silica were exposed to selected alumination conditions in NaOH. Like for SBA-15, treatment of the ordered silicas COK-12 and MCM-41 (**Table S2**) resulted in a yield of about 75%, which increased to about 100% with an increased $[Al]_{initial}$. Additionally, for these materials the base-only treatment leads to a reduction of the overall BET surface area, and an enlarged average pore diameter (d_p) (**Figure S5**). Similar to the yield, these effects decreased with increased $[Al]_{initial}$.

For non-ordered amorphous silica (AS1-P and AS2-P), the weight loss at low $[Al]_{initial}$ was about two-fold (ca. 50%, **Table 1**, **Figure 2a**). Intuitively, the reactivity of silica towards alkaline media may be directly related to its overall (BET) surface area. However, the degree of dissolution in the absence of aluminum does not relate well with the total BET surface area (**Table 2**). Nevertheless, a trend was attained between the treatment solid mass yield (Y) and the pore size of the parent silica (**Figure S6**), suggesting a minimum (meso)pore size to achieve a larger extent of dissolution. This implies that, under the studied conditions, the higher solid yields of the ordered silica may be caused by the limited access of the base hydroxyls to the center part of the unidirectionally structured MCM-41, SBA-15, and COK-12 particles. This hypothesis agrees well with the local reduction at the edges of the SBA particles as evidenced by TEM (*vide supra*). Alike SBA-15, for high $[Al]_{initial}$ high yields (up to 100%) were attained for the non-ordered silica, whereas the porosity was largely preserved. In dried silica gel-derived samples ('AS1-*x*-b') the pore size distributions remained almost unchanged with only slightly larger tail towards larger pore sizes (**Figure 3d**). Typical pore sizes occurred between 5 and 20 nm with a maximum around 10 nm. On the other hand, fumed silica-derived samples ('AS2-*x*-b'), displayed a more pronounced increase in the number of larger mesopores after alumination (25-35 nm, **Figure S5d**).

The treatments successfully introduced substantial Brønsted and Lewis acidity into the materials. About 30% lower acidities were obtained compared to SBA-15 (**Table 2**). The

This article is protected by copyright. All rights reserved.

Accepted Manuscript

AS1-derived samples typically displayed about 40-50% lower B/L ratios compared to SBA-15-derived samples, and, in this regard, the acidic properties are closer to the commercial standard ASA materials.[8,9,28] Compared to the acidities of these commercial materials (ASA-6 and ASA-0.4), the total acidities of ~60 μmol g^{-1} obtained for the AS1 and AS2 samples are slightly lower. Still, AS1 and AS2-based samples feature considerably higher Si/Al ratios (based on the maximal theoretical amount of incorporated aluminum), and therefore should display substantially higher effective acidities (**Table 2**). Moreover, optimizations on the alumination of these amorphous silicas may further enhance the acidity of these materials. Finally, in-line with the SBA-15-related materials, hydrothermal treatment of AS1-0.03-NaOH yielded a preservation of the BET surface area.

2.4. Catalytic Functionality

The functionality of the formed acid sites in selected samples was evaluated in several acid-catalyzed reactions (**Figure 7**). These regard reactions involving substrates of different sizes catalyzed by either Lewis, Brønsted, or both types of acid sites, therefore enabling a thorough insight in the catalytic potential of the aluminosilicate catalysts. The Friedel-Crafts alkylation of toluene with benzyl alcohol (BA) is catalyzed by moderate and strong Brønsted acid sites (**Figure 7a-b**), and represents a frequently-used model reaction for acid catalysis in the condensed phase.[29] An increase of the conversion of benzyl alcohol (A_{BA}) was observed for increasing $[Al]_{initial}$ in NaOH-treated SBA-15 (S-*x*-NaOH, **Figure 7a**). On the other hand, the S-*x*-NH_4OH samples display an optimum in A_{BA} of 19 $mmol_{BA}$ g_{cat}^{-1} h^{-1} at $[Al]_{initial}$ = 0.02 M. Aluminations with $NaAlO_2$ enhance the activity with increasing $[Al]_{initial}$, however, this enhancement is smaller compared to the S-*x*-NaOH samples. For example, the maximum activity (S-0.03-$NaAlO_2$) was around 75% compared to S-0.03-NaOH. S-0.03-H_2O and S-0.04-NaOH performed poorly showing an activity of about 10 $mmol_{BA}$ g_{cat}^{-1} h^{-1}, further highlighting the importance of optimizing the Al concentration in the alumination process.

This article is protected by copyright. All rights reserved.

Accepted Manuscript

Based on the performance of the S-*x*-b samples, several AS-1-derived samples were selected for catalytic evaluation. AS1-0.03-NaOH and AS1-0.02-NH_4OH samples displayed an A_{BA} of 15 and 16 $mmol_{BA}\ g_{cat}^{-1}\ h^{-1}$, which is slightly higher than for commercial ASA-6 (14 $mmol_{BA}\ g_{cat}^{-1}\ h^{-1}$), and significantly higher compared to γ-alumina (2 $mmol_{BA}\ g_{cat}^{-1}\ h^{-1}$). Otherwise, the sample AS1-0.015-$NaAlO_2$ resulted in an activity of 9 $mmol_{BA}\ g_{cat}^{-1}\ h^{-1}$. An approximately linear relation was found between Brønsted acidity and A_{BA} for Brønsted acidities below 30 μmol g^{-1} (**Figure 7b**). In general, the aluminated samples displayed a higher performance per Brønsted acid site compared to ASA-6, suggesting that the acid sites (particularly in the S-*x*-NaOH samples) offer higher functionality.

The catalytic pyrolysis of low-density polyethylene (LDPE) -an important challenge in the repurposing of plastic waste- was applied as model reaction to evaluate the ability of the catalyst to convert high molecular-weight hydrocarbons (**Figure 7e-f**).[30-31] The LDPE pyrolysis was studied by comparing the temperature where 50% (T_{50}) of the mass was converted to volatile products. **Figure 7e** shows T_{50} decreasing as a function of the applied initial aluminum concentration down to 375 °C for an $[Al]_{initial}$ of 0.02 M. At higher aluminum concentrations, the T_{50} remained largely constant for the S-0.03-NH_4OH and S-0.03-$NaAlO_2$ samples. In contrast, for S-0.03-NaOH, the T_{50} decreases to about 336 °C. The latter conversion is lower compared to the commercial, strongly-acidic USY zeolites with Si/Al ratio of 40 (USY-40) and 2.6 (USY-2.6), which reached a T_{50} of 341 °C and 377 °C, respectively. T_{50} values of non-ordered AS1 samples after alumination were comparable (*ca.* 360 °C) to the commercial amorphous aluminosilicate ASA-6. An inverse correlation was visible between T_{50} and the total acidity (**Figure 7f**). Based on the lower position of the profile, like in the case of the aforementioned alkylation, the acid sites in the S-*x*-NaOH samples seem to achieve the most efficient catalytic performance.

The aluminated samples were also tested in the reaction of 1,3-dihydroxyacetone (DHA) to ethyl lactate (ELA) via pyruvic aldehyde (PAL) (**Figure 7g-h**). Lactic acid (and its ester

This article is protected by copyright. All rights reserved.

Accepted Manuscript

derivatives, such as ELA) is emerging as a renewable chemical platform for solvents, acrylic acid and poly-lactic acid, an important biodegradable plastic.[32-35] Often the rate-determining step in the conversion of DHA to ELA is the dehydration and subsequent rearrangement of DHA to PAL, which is catalyzed by both Brønsted and Lewis acid sites. The second step, PAL to ELA with incorporation of ethanol solvent, is catalyzed primarily by Lewis acid sites at low temperature, while strong Brønsted acidity leads to side products and low product selectivity.[32] The initial rate ELA formation (R_{ELA}) showed that the S-0.03-NaOH sample was most active, plotted in function of $[Al_{initial}]$ (**Figure 7g**), *e.g.* yielding 15% of ELA after 1 h compared to 9% and 13% in S-0.03-$NaAlO_2$ and ASA-6, respectively. Other alumination techniques showed lower ELA formation rates. A roughly linear relation was observed between the R_{ELA} and the total amount of acid sites (**Figure 7h**). The latter suggest that the Lewis acid sites in the materials are active in the conversion of PAL to ELA, as the sole activity Brønsted acid sites would have resulted in a much higher selectivity to side-products at the expense of ELA formation.[32]

The valorization of α-pinene was used as a second test reaction in the field of bio-based renewables (**Figure 7c-d**). α-pinene is the main component of turpentine oil, which is a significant side product in the paper and the medium density fiberboard industry, which both use (pine) trees as biomass source.[36] In this reaction, the rate determining step is based on the Brønsted acid catalyzed conversion of α-pinene to the pinanyl carbocation, that further rearranges into mono- and bicyclic products. Fast product diffusion (and thus acidity in large accessible pores) is essential to avoid polymeric hydrocarbon formation. The activity ($A_{\alpha\text{-}p}$) and showed an optimum around $[Al]_{initial}$ of 0.015 M, where activities of *ca.* 400 $mmol_{\alpha\text{-}p}\ g_{cat}^{-1}\ h^{-1}$ are reached (**Figure 7c**). The latter indicates that, for this reaction, an optimum of acidity exist for the aluminated samples. The activity and productivity of the aluminated MCM-41 (M-*x*-NaOH) samples showed roughly similar performance compared to the S-*x*-NaOH samples, yielding an activity of ~400 $mmol_{\alpha\text{-}p}\ g_{cat}^{-1}\ h^{-1}$ at $[Al]_{initial}$ = 0.02 M.

This article is protected by copyright. All rights reserved.

Accepted Manuscript

Finally, selected aluminated samples were tested in the cracking (dealkylation) reaction of propyl phenol. The cracking of alkylated aromatics plays an important role in modern day petroleum refineries, and is likely to gain high attention in future bio-refineries. This reaction is catalyzed by Brønsted and Lewis acid sites in gas phase, but zeolites are required to achieve high phenol selectivity (>90%).[37] The aluminated materials were active in the dealkylation of propylphenol (**Figure 8**). S-*x*-b samples display similar conversions of propylphenol (X_{pp}) compared to the sample ASA-6, whereas AS1-*x*-b samples resulted in slightly lower conversions (**Figure 8a,b**). The samples aluminated with $NaAlO_2$ systematically displayed the lowest X_{pp}. Despite the lower conversions compared to ASA-6, the selectivity towards phenol and propylene (S_{da} in **Figure 8c,d**) was about 15% higher for the AS1-*x*-*b* samples. S-*x*-b samples also displayed higher selectivities than ASA-6, comparable to the AS1-*x*-b samples. The highest S_{da} was achieved in the AS1-0.03-NaOH (S_{da}~90%, at X_{pp}~70%). This sample approached the very high shape selectivity of the zeolite ZSM-5 (> 95%) which is remarkable, given its amorphous nature and inexpensive synthesis.

2.5. Relationship between solid, pH, acidity, and activity

The implications of aluminations of silica should not only be evaluated by the used aluminum and silica source, but also by the involved pH (**Figure 9a**). Herein, the use of base additives can play an important role, as they allow tailoring of the pH to that point, at which the Al is most efficiently deposited on the external surface of silica. In addition to the initial pH of the alumination solution, the pH development during the treatment also matters. In fact, the pH at the end of the treatments (pH_{final}, **Table S3**) may be even more important, as judged by the volcano-type relation of both the total acidity (B+L) and the activity in alkylation to the pH_{final} (**Figure 9b**). Both quantities are optimal when pH_{final} is neutral (pH 5-8). Hence, if the pH strongly varies in time during the alumination (as with strong bases such as NaOH, **Figure 1b**), control of the treatment time becomes important. In this context, weak bases, such as

This article is protected by copyright. All rights reserved.

Accepted Manuscript

NH_4OH (**Figure 1c**), provide the additional advantage that the pH during the treatment can be buffered and more easily controlled. In addition, using the latter base enables to obtain the active protonic form of the catalysts by a single calcination step, and makes the otherwise-required ion exchange obsolete.

3. Conclusions

Despite the extended history of the synthesis and application of amorphous silica-alumina, the role of the pH in the post-synthetic alumination of silica materials has never been studied. We demonstrated within this contribution that by decoupling the pH from the Al concentration in post-synthetic alumination of silica, unique aluminosilicate catalysts at high solid yields are obtained. In a case study on widely-studied SBA-15, materials with preserved porosity, unprecedented acidities, superior hydrothermal stability and superior catalytic performance were prepared. The catalytic diversity of controlled aluminations was shown in several acid-catalyzed reactions (toluene alkylation, α-pinene isomerization, alkylphenol dealkylation, and ethyl lactate synthesis), where the materials outperformed established amorphous aluminosilicate materials. Moreover, in the pyrolysis of LDPE plastics an enhanced performance compared to both amorphous and crystalline aluminosilicates (zeolites) was demonstrated. The developed pathways can be applied to any porous silica, as we have verified by preparing aluminosilicate catalysts from several other ordered and non-ordered amorphous silica sources. The presented synthetic insights open the door to the synthesis, in-depth characterization, and application of a novel family of amorphous aluminosilicate materials, in which a more efficient use of aluminum ensures an enhanced activity, selectivity, and stability in catalytic conversions.

4. Experimental Section

This article is protected by copyright. All rights reserved.

Accepted Manuscript

Synthesis of ordered silicas: SBA-15 was synthesized as stated in literature.[25] 20.0 g of Pluronic P123 (Sigma-Aldrich) was dissolved in 635 g distilled H_2O and 115 g concentrated HCl (Fisher) (37 wt.%) at 35 °C. After a full P123 dissolution 43 g of tetraethyl orthosilicate (TEOS, Acros) was added for synthesis of ~12 g of silica. This mixture was stirred for 20 h at 35 °C and afterwards filtered and washed. The recovered powder was dried overnight at 80 °C and finally calcined at 550 °C for 6 h (ramp rate: 1 °C min^{-1}). The synthesis procedures of other ordered mesoporous silica MCM-41 and COK-12 are described in the supporting information (**Table S2**). Parent materials are denoted as 'a-P'. Herein 'a' is the type of parent material: 'S' for SBA-15, 'M' for MCM-41 and 'C' for COK-12. The 'P' indicates that it regards the parental untreated silica.

Commercial silicas and aluminosilicates: Two commercial amorphous (non-ordered) silicas were used as parent material: silica gel (6 nm pore size, 230-400 mesh particle size, 40-63 µm particle size; Sigma-Aldrich, denoted as 'AS1-P') and fumed silica (Aerosil 380, denoted as 'AS2-P'). Several commercial aluminosilicate references for acidity and catalytic benchmarks were used: amorphous silica alumina (Grace, Si/Al=6, denoted as ASA-6'), USY zeolite CBV-780 (Zeolyst, Si/Al=40, denoted as 'USY-40'), and USY zeolite CBV-600 (Zeolyst, Si/Al=2.6, denoted as 'USY-2.6'). In the case of these aluminosilicates the number in the label corresponds to their Si/Al ratio.

Post-synthetic aluminations: Aluminations were performed at room temperature by adding 10 ml solutions of distilled water, or 0.1 M sodium hydroxide (Fisher), or 0.5 M ammonium hydroxide (Chemlab) to 0.333 g of silica source and the appropriate amount of $Al(NO_3)_3 \cdot 9H_2O$ (Chemlab) or $NaAlO_2$ (Sigma Aldrich), followed by stirring (300 rpm) for 30 min. In the case of aluminations with NaOH and NH_4OH, $Al(NO_3)_3 \cdot 9H_2O$ was used. Aluminations with $NaAlO_2$ were performed in the absence of an additional base. After the alumination, samples were immediately suspended in 400 ml H_2O, followed by a filtering and washing step. The recovered powder was dried overnight at 80 °C and calcined at 550 °C for

This article is protected by copyright. All rights reserved.

Accepted Manuscript

6 h (ramp rate: 1°C min^{-1}). The mass yields after alumination were calculated by dividing the final mass after calcination by the product of the mass before alumination (0.333 g) and the maximal amount of Al_2O_3 incorporated in the solid based on the applied aluminum concentration (up to 0.040 g). The samples were converted to the protonic form by three consecutive NH_4^+-ion exchanges of 6 h (1 g of silica per 100 ml NH_4NO_3 (Acros) solution of 0.1 M) with intermediate filtering and washing followed by a calcination as described above. The hydrothermal stability of the selected samples was assessed by refluxing the solids (100 mg) in a round-bottom flask (100 ml) filled with distilled water (10 mL) at 100 °C for 22 h. After treatment, solids were isolated by Büchner funnel filtration, followed by washing and drying overnight at 60°C.

Sample coding after aluminations: Samples were labeled by the generic formula 'a-*x*-b'. The 'a' refers to the used starting silica source. In the case no silica was added in the alumination solution (**Figure 1a**), the 'a' is substituted with a '0'. The '*x*' in 'a-*x*-b' refers to the initial concentration of Al in the alumination solution ($[Al]_{initial}$ in mol l^{-1}). Finally, 'b' refers to the type of base used in the alumination: 'NaOH' for aluminations in aqueous NaOH, 'NH_4OH' for aluminations in aqueous NH_4OH, and '$NaAlO_2$' for aluminations with $NaAlO_2$ in distilled water. In the case no alkaline source was present, *i.e.* aluminations with $Al(NO_3)_3{\cdot}9H_2O$ in distilled water, 'b' was replaced with 'H_2O'. For example, SBA-15 treated in a 0.1 M NaOH solution with 0.006 M $Al(NO_3)_3{\cdot}9H_2O$ is denoted as 'S-0.006-NaOH'. Similarly, SBA-15 aluminated in distilled water complemented with 0.03 M of $Al(NO_3)_3{\cdot}9H_2O$ is referred to as 'S-0.03-H_2O'. Finally, silica gel treated in distilled water complemented with 0.02 M of $NaAlO_2$ is referred to as 'AS1-0.02-$NaAlO_2$'. An additional overview of the sample nomenclature is provided in **Table S4**.

Characterization: Nitrogen physisorption isotherms were determined using a Tristar 3000 (Micromeritics) at -196 °C. Samples were degassed prior to analysis under N_2 flow at 300 °C overnight. Pore size distributions (PSDs) were determined using the NL-DFT (non-local

Accepted Manuscript

This article is protected by copyright. All rights reserved.

density functional theory) model for cylindrical pores in metal oxides for the adsorption isotherm.[38] The standard deviations on the model were between 2 and 5 cm^3 g^{-1}. Specific surface areas were determined using the BET model (Brunauer, Emmett, Teller).

Transmission electron microscopy (TEM) was carried out on a FEI Tecnai F30 with a field emission gun at 300 kV. Prior to analysis, samples were dispersed in ethanol and dropped onto a copper grid with a lacey carbon layer. For image processing the program Digital Micrograph (Gatan Inc.) was used.

Bulk Si and Al contents (Si_{ICP}/Al_{ICP}) were determined using inductively coupled plasma optical emission spectroscopy (ICP-OES) using analytical wavelengths of λ = 251.611 nm for Si and λ = 396.153 nm for Al on a Varian 720-ES instrument. 50 mg of the samples was mixed with 250 mg $LiBO_2$ and heated for 10 min at 1000 °C. The molten material was then dissolved in 0.42 M HNO_3 and further diluted. The water content in the material was measured on several accounts and an average of 10 wt.% was taken into account for determination of the Al and Si content.

Surface Si and Al contents (Si_{XPS}/Al_{XPS}) were probed with X-ray photoelectron spectroscopy (XPS) using a Specs Phoibos 100 with Mg K_α radiation (1253.6 eV) at 300 W in an energy range of 0 – 1000 eV. The spectrometer is equipped with a hemispherical analyzer allowing high sensitivity and high resolution experiments. Energy scale and binding energy were calibrated with Cu and Au foils at the binding energies of Cu $2p_{3/2}$ (932.67 eV) and Au $4f_{7/2}$ (84.00 eV), respectively. Because of large gas adsorption, the sample chamber could only be held at a base pressure of around $3 \cdot 10^{-8}$ mbar after 1 h of pumping to degas the samples in a pre-vacuum chamber. Spectra were acquired with a pass energy of 15 eV and a step size of 0.1 eV. The spectra were analyzed with the software CASA-XPS and the element concentrations are calculated with the standard sensitivity factors provided by the software.

^{27}Al magic angle spinning (MAS) NMR spectra were collected using a Bruker Avance III 400 MHz spectrometer equipped with a 9.4 T wide-bore magnet operating at a Larmor frequency

This article is protected by copyright. All rights reserved.

Accepted Manuscript

of 104.3 MHz. The samples were hydrated for 48 h over a saturated salt solution prior to analysis and packed in 4-mm ZrO_2 MAS rotors. ^{27}Al MAS NMR spectra were recorded in a double resonance probe at a spinning rate of 14 KHz. Spectra were obtained using a $\pi/18$ short rf pulse (~0.3 μs) calibrated using an aqueous solution of $Al(NO_3)_3$, corresponding to an rf field strength of 104 kHz. The recycle delay was set to 1 s and the number of scans was between 10 k and 30 k. Chemical shifts are quoted in ppm from the aqueous solution of $Al(NO_3)_3$ (0 ppm).

Pyridine-probed Fourier transformed infrared (PP-FTIR) spectroscopy was executed using a Nicolet 6700 spectrometer equipped with a DTGS detector. Samples were pressed into self-supporting plates and degassed at 400 °C for 1 h in vacuum before measurements. Lewis and Brønsted acid sites were analyzed using a pyridine probe. After evacuation, the samples were saturated by 4–5 pulses of ~25 mbar of pyridine at 50 °C for 1 min. Physisorbed pyridine was removed by heating to 150 °C. The spectra were collected at 150 °C after 20 min of equilibration. The absorptions at 1450 and 1550 cm^{-1} correlated to the amount of Lewis (L) and Brønsted (B) acid sites, respectively. The extinction coefficients used were similar to those determined by Emeis.[39]

Catalysis: Alkylations of toluene with benzyl alcohol were performed by mixing 0.025 g of catalyst with 4.98 ml (47 mmol) toluene (Fisher), 0.062 ml (0.6 mmol) benzyl alcohol (Sigma Aldrich) and 0.048 ml (0.3 mmol) propyl cyclohexane (TCI Europe) as internal standard. The catalyst powder was predried for 2 h at 300 °C (ramp 5 °C min^{-1}) and the reaction was carried out in closed Schott bottles (Duran) for 1 h under stirring at 120 °C. The reaction mixture was analyzed with gas chromatography (Agilent 6850 series).

Low density polyethylene (Alfa Aesar, particle size = 500 μm, density = 0.92 g cm^{-3}) catalytic cracking was carried out in thermogravimetric analysis (TGA, Q500 TA Instruments). The powdered polymer (6 mg) and catalyst (2 mg) were carefully weighed in a TGA crucible and

This article is protected by copyright. All rights reserved.

Accepted Manuscript

suitably mixed in order to obtain an intimate contact. The reaction was performed in N_2 flow (70 cm^3 min^{-1}) ramping the temperature from room temperature to 700 °C with 10 °C min^{-1}.

The isomerization of α-pinene (Sigma-Aldrich) was carried out in a 50 ml Parr reactor with a sampling device at 150 °C under 6 bar of nitrogen with a stirring speed of 750 rpm. A mixture of substrate (20 g α-pinene) and catalyst (0.4 g) was heated to 100 °C, the first liquid sample was taken subsequently. The reaction mixture was then further heated to 150 °C and more samples were taken 10, 30, and 60 min after the first sample. All samples were analyzed on a gas chromatograph (5890, Hewlett Packard) equipped with an HP1 column and a flame ionization detector. Tetradecane (Sigma-Aldrich) was used as an external standard. Activity ($A_{\alpha\text{-}p}$) was determined by using the slope of the linear part of the conversion of α-pinene *versus* the contact time.

For the synthesis of ethyl lactate (ELA, Sigma-Aldrich), 5 ml ethanol (Fisher) solutions with 0.4 M 1,3-dihydroxyacetone (Sigma-Aldrich) and naphthalene (internal standard, Alfa-Aesar) were added to 0.2 g of catalyst. The reaction was performed in glass crimp cap vials at 110 °C under stirring. The reaction mixture was analyzed with a gas chromatograph (Agilent 6850 series) equipped with an FID detector and a 30 m Agilent HP-5 column,. A calibration curve versus naphthalene was used for the response factor. Initial rates of ELA formation (R_{ELA}) were determined by using the slope of the linear part of the ELA yield *vs.* contact time, assessed at < 21% yield.

Dealkylation experiments were performed in a custom-built plug-flow fixed-bed reactor equipped with 4 parallel quartz reactors (inner diameter of 3 mm). Typically, the quartz reactors were filled with in total 120 mg of catalysts (sieve fraction: 0.125–0.250 mm), yielding a catalyst bed height of ca. 13 mm. Propyl phenol (Sigma-Aldrich, >97%) and water were brought to the gas phase using a nitrogen flow (20 ml min^{-1}) passed through a saturator. Afterwards these flows were mixed, yielding a gas mixture of the molar composition 0.86/0.12/0.02 (N_2/H_2O/alkylphenol), and passed through the reactors. Effluent gases were

This article is protected by copyright. All rights reserved.

Accepted Manuscript

characterized using an in-line gas chromatograph (Agilent 6850 series) equipped with a HP1 column and a FID detector.

Supporting Information

Supporting Information is available from the Wiley Online Library or from the author.

Acknowledgements

D. V. and M. D. acknowledge support from an FWO post-doctoral fellowship. R. L. acknowledges the IAP. N. N. acknowledges the KU Leuven (FLOF). L. M. thanks CICECO-Aveiro Institute of Materials, POCI-01-0145-FEDER-007679 (FCT Ref. UID /CTM / 50011/2013 and PTDC/QEQ-QAN/6373/2014), financed by national funds through the FCT/MEC and when appropriate co-financed by FEDER under the PT2020 Partnership Agreement. The authors are also grateful to the Portuguese NMR Network (RNRMN).

Received: ((will be filled in by the editorial staff))
Revised: ((will be filled in by the editorial staff))
Published online: ((will be filled in by the editorial staff))

References

[1] G. Busca, *Chem. Rev.* **2007**, *107*, 5366-5410.
[2] W. Vermeiren, J.-P. Gilson, *Top. Catal.* **2009**, *52*, 1131-1161.
[3] J. A. Scherzer, A. J. Gruia, in *Hydrocracking Science and Technology*, Marcel Dekker, New York, **1996**, p. 215.
[4] C. Pistarino, E. Finocchio, M. A. Larrubia, B. Serra, S. Braggio, G. Busca, M. Baldi, *Ind. Eng. Chem. Res.* **2001**, *40*, 3262-3269.
[5] R. Mann, *Catal. Today* **1993**, *18*, 509-528.
[6] E. Garrone, F. Fajula, in *Acidity and Basicity* (Eds.: H. G. Karge, J. Weitkamp), Springer-Verlag Berlin Heidelberg, **2008**.
[7] G. Busca, in *Metal Oxides* (Ed.: J. L. G. Fierro), CRC Press, **2005**, pp. 247-318.
[8] E. J. M. Hensen, D. G. Poduval, P. C. M. M. Magusin, A. E. Coumans, J. A. R. van Veen, *J. Catal.* **2010**, *269*, 201-218.
[9] T. C. Keller, J. Arras, M. O. Haus, R. Hauert, A. Kenvin, J. Kenvin, J. Pérez-Ramírez, *J. Catal.* **2016**, *344*, 757-767.
[10] V. C. F. Holm, G. C. Bailey, A. Clark, *J. Phys. Chem.* **1959**, *63*, 129-133.
[11] M. Caillot, A. Chaumonnot, M. Digne, J. A. Van Bokhoven, *ChemCatChem* **2014**, *6*, 832-841.
[12] M. Caillot, A. Chaumonnot, M. Digne, C. Poleunis, D. P. Debecker, J. A. van Bokhoven, *Microp. Mesop. Mater.* **2014**, *185*, 179-189.
[13] R. Mokaya, W. Jones, Z. Luan, M. Alba, J. Klinowski, *Catal. Lett.* **1996**, *37*, 113-120.
[14] L. Y. Chen, Z. Ping, G. K. Chuah, S. Jaenicke, G. Simon, *Microp. Mesop. Mater.* **1999**, *27*, 231-242.
[15] R. Mokaya, W. Jones, *J. Mater. Chem.* **1999**, *9*, 555-561.
[16] Z. Luan, M. Hartmann, D. Zhao, W. Zhou, L. Kevan, *Chem. Mater.* **1999**, *11*, 1621-1627.
[17] S. Biz, M. G. White, *J. Phys. Chem. B* **1999**, *103*, 8432-8442.
[18] K. G. Miesserov, *Russ. Chem. Bull.* **1956**, *5*, 1207-1211.

This article is protected by copyright. All rights reserved.

Accepted Manuscript

[19] H.-M. Kao, C.-C. Ting, S.-W. Chao, *J. Mol. Catal. A.* **2005**, *235*, 200-208.
[20] R. Locus, D. Verboekend, R. Zhong, K. Houthoofd, T. Jaumann, S. Oswald, L. Giebeler, G. Baron, B. F. Sels, *Chem. Mater.* **2016**, *28*, 7731-7743.
[21] C. J. Brinker, G. W. Scherer, *Sol-gel Science: The Physics and Chemistry of Sol-gel Processing*, Academic Press, San Diego, **1990**.
[22] J. Van Aelst, *et al.*, *Adv. Funct. Mater.* **2015**, *25*, 7130-7144.
[23] D. Zhai, L. Zhao, Y. Liu, J. Xu, B. Shen, J. Gao, *Chem. Mater.* **2015**, *27*, 67-74.
[24] D. Verboekend, J. Pérez-Ramírez, *Chem. Eur. J.* **2011**, *17*, 1137-1147.
[25] D. Zhao, Q. Huo, J. Feng, B. F. Chmelka, G. D. Stucky, *J. Am. Chem. Soc.* **1998**, *120*, 6024-6036.
[26] T. Ennaert, J. Geboers, E. Gobechiya, C. M. Courtin, M. Kurttepeli, K. Houthoofd, C. E. A. Kirschhock, P. C. M. M. Magusin, S. Bals, P. A. Jacobs, B. F. Sels, *ACS Catal.* **2015**, *5*, 754-768.
[27] R. Mokaya, *J. Phys. Chem. B*, **2000**, *104*, 8279–8286 .
[28] E. J. M. Hensen, D. G. Poduval, V. Degirmenci, D. A. J. M. Ligthart, W. Chen, F. Maugé, M. S. Rigutto, J. A. R. van Veen, *J. Phys. Chem. C* **2012**, *116*, 21416-21429.
[29] D. Verboekend, M. Milina, S. Mitchell, J. Pérez-Ramírez, *Cryst. Growth Des.* **2013**, *13*, 5025-5035.
[30] J. Pérez-Ramírez, S. Abelló, A. Bonilla, J. C. Groen, *Adv. Funct. Mater.* **2009**, *19*, 164-172.
[31] D. W. Park, E. Y. Hwang, J. R. Kim, J. K. Choi, Y. A. Kim, H. C. Woo, *Polym. Degrad. Stab.* **1999**, *65*, 193-198.
[32] F. de Clippel, M. Dusselier, R. Van Rompaey, P. Vanelderen, J. Dijkmans, E. Makshina, L. Giebeler, S. Oswald, G. V. Baron, J. F. M. Denayer, P. P. Pescarmona, P. A. Jacobs, B. F. Sels, *J. Am. Chem. Soc.* **2012**, *134*, 10089-10101.
[33] P. P. Pescarmona, K. P. F. Janssen, C. Delaet, C. Stroobants, K. Houthoofd, A. Philippaerts, C. De Jonghe, J. S. Paul, P. A. Jacobs, B. F. Sels, *Green Chem.* **2010**, *12*, 1083-1089.
[34] J. Dijkmans, M. Dusselier, D. Gabriëls, K. Houthoofd, P. C. M. M. Magusin, S. Huang, Y. Pontikes, M. Trekels, A. Vantomme, L. Giebeler, S. Oswald, B. F. Sels, *ACS Catal.* **2015**, *5*, 928-940.
[35] M. Dusselier, P. Van Wouwe, A. Dewaele, E. Makshina, B. F. Sels, *Energy Environ. Sci.* **2013**, *6*, 1415-1442.
[36] N. Nuttens, D. Verboekend, A. Deneyer, J. Van Aelst, B. F. Sels, *ChemSusChem* **2015**, *8*, 1197-1205.
[37] D. Verboekend, Y. Liao, W. Schutyser, B. F. Sels, *Green Chem.* **2016**, *18*, 297-306.
[38] M. Jaroniec, M. Kruk, J. P. Olivier, S. Koch, in *Stud. Surf. Sci. Catal., Vol. 128* (Eds.: G. Kreysa, J. P. Baselt, K. K. Unger), Elsevier, **2000**, pp. 71-80.
[39] C. A. Emeis, *J. Catal.* **1993**, *141*, 347-354.

Accepted Manuscript

This article is protected by copyright. All rights reserved.

10.1002/cctc.201701660

WILEY-VCH

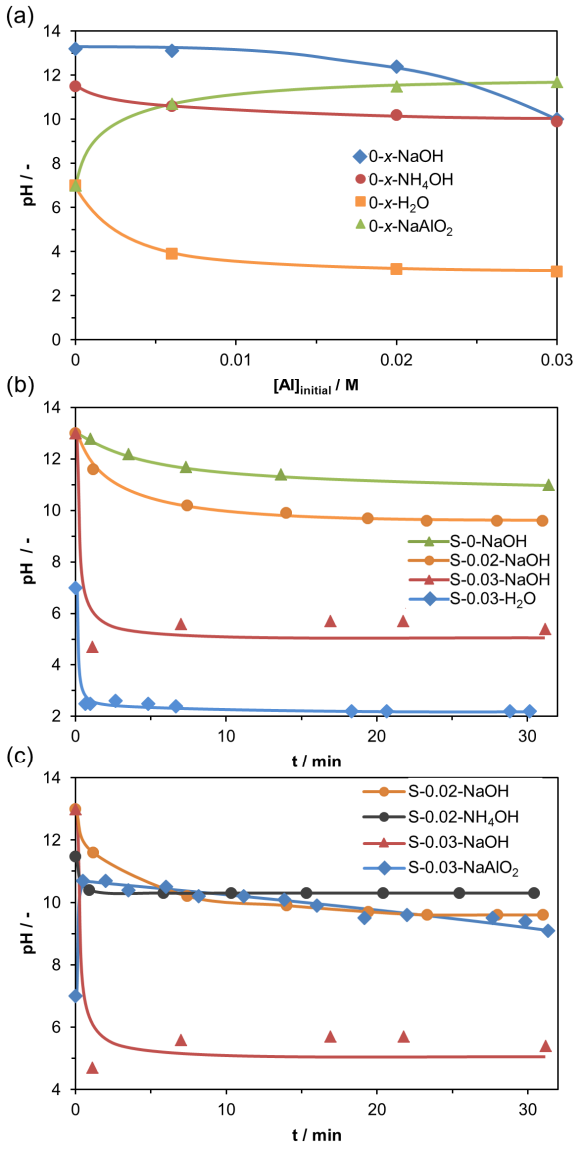

Figure 1. (a) Measured pH values in aqueous solutions of different Al sources, with and without base addition such as NaOH (0-*x*-NaOH), $NaAlO_2$ (0-*x*-$NaAlO_2$), or NH_4OH (0-*x*-NH_4OH). The '*x*' refers to the applied concentration of aluminum ($[Al]_{initial}$). (b,c) pH evolution during aluminations of SBA-15. In the case H_2O, NaOH, or NH_4OH is used in a synthesis or solution, $[Al]_{initial}$ refers to the $Al(NO_3)_3$ concentration. Conversely, in the case $NaAlO_2$ is used, $Al(NO_3)_3$ is not used and $[Al]_{initial}$ refers to the $NaAlO_2$ concentration.

This article is protected by copyright. All rights reserved.

Accepted Manuscript

Table 1. Mass yields, composition, and porous properties of parental and aluminated silica.

Sample	Yield[a] (%)	Si/Al[b] (mol mol^{-1})	S_{BET}[c] ($m^2 g^{-1}$)	d_{pore}[d] (nm)	V_{pore}[e] ($cm^3 g^{-1}$)
S-P	100	no Al	679 (-36%)[g]	7	0.63
S-0-NaOH	77	no Al	352	8	0.46
S-0.002-NaOH	80	243 (45)	327	8	0.57
S-0.006-NaOH	82	81 (-)	301	7	0.50
S-0.015-NaOH	91	39 (21)	292	6	0.44
S-0.02-NaOH	89	30 (14)	308	7	0.41
S-0.03-NaOH	100	20 (15)	497 (+2%)	7	0.51
S-0.04-NaOH	100	-	770	7	0.72
S-0.03-H_2O	97	-	418	6	0.43
S-0.006-NH_4OH	87	87	404	8	0.56
S-0.02-NH_4OH	94	29	354 (+1%)	7	0.46
S-0.03-NH_4OH	95	19	340	7	0.43
S-0.006-$NaAlO_2$	95	137	465	8	0.53
S-0.015-$NaAlO_2$	94	54	413 (+10%)	7	0.48
S-0.02-$NaAlO_2$	95	41	408	7	0.48
S-0.03-$NaAlO_2$	97	-	364	7	0.46
AS1-P	100	-	473 (-37%)	10	0.74
AS1-0.006-NaOH	51	81[h]	395	12	0.76
AS1-0.02-NaOH	74	30[h]	375	10	0.61
AS1-0.03-NaOH	100	22[h]	370 (+2%)	10	0.69
AS1-0.02-NH_4OH	99	29[h]	321	12	0.60
AS1-0.015-$NaAlO_2$	97	55[h]	387	12	0.74
AS2-P	100	-	316	26	0.55
AS2-0.006-NaOH	52	81[h]	239	32	1.08
AS2-0.015-NaOH	83	41[h]	262	32	1.13
AS2-0.03-NaOH	90	22[h]	237	32	0.99
ASA-6	-	6	403 (-16%)	26	1.24

[a]Mass yield after alumination divided by mass before alumination combined with the maximal amount of Al_2O_3 incorporated. [b]Si/Al ratio of the bulk (Si_{ICP}/Al_{ICP}) and the surface (Si_{XPS}/Al_{XPS}, the latter between brackets). [c]Specific surface area (BET method). [d]Average pore diameter(s) on the basis of the adsorption NL-DFT pore size distribution. [e]Total pore volume. [c-f]N_2 physisorption. [g]The values in brackets indicate the change in BET surface area after a hydrothermal treatment (conditions in the experimental section).[h]Values were not measured, but calculated assuming the Al incorporation was the same (91%) as in the corresponding SBA-15 samples (following **Figure 2c**).

This article is protected by copyright. All rights reserved.

Accepted Manuscript

WILEY-VCH

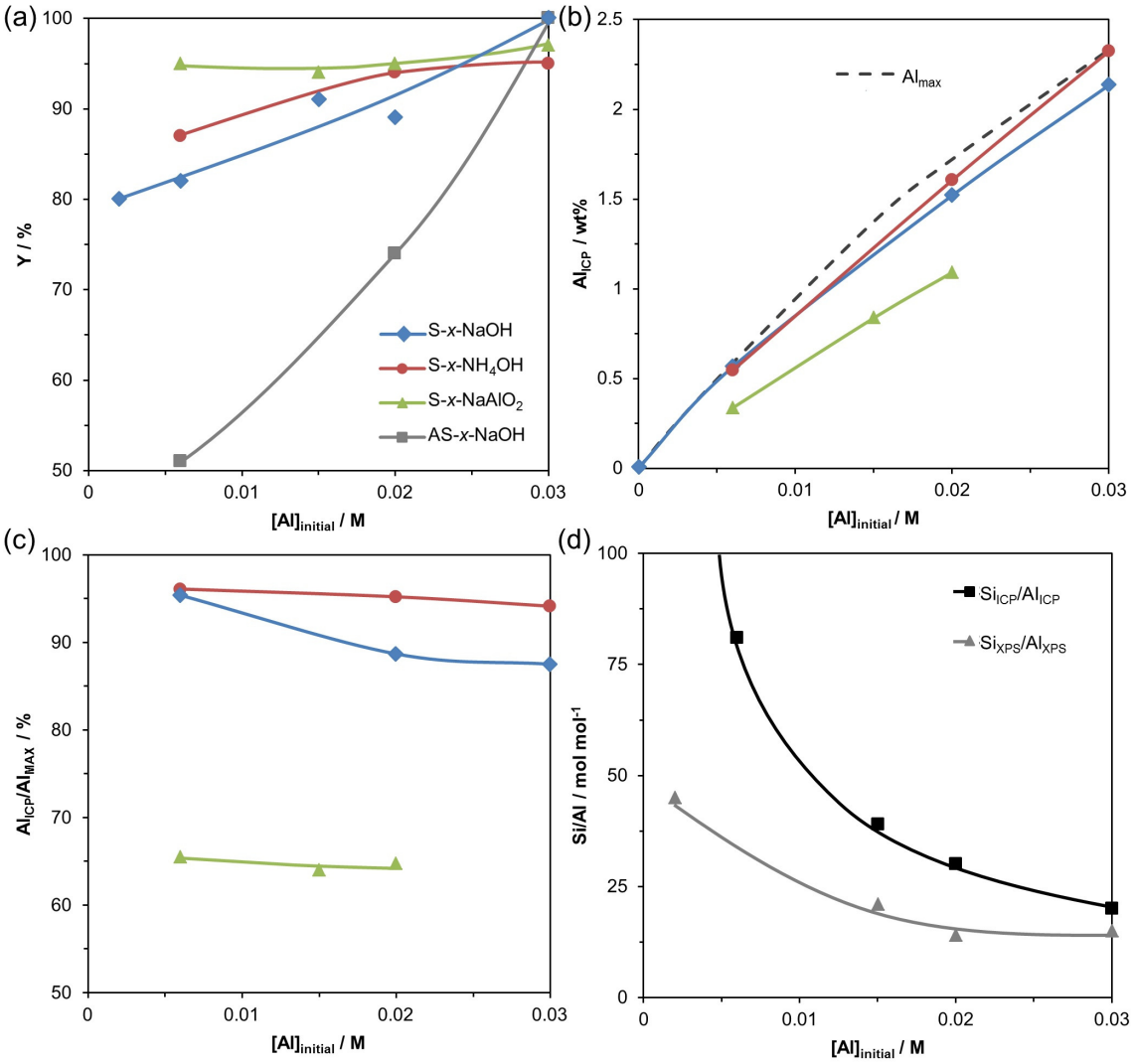

Figure 2. (a) Mass yields (Y) after alumination of SBA-15 (S-*x*-b) and amorphous silica (AS1-*x*-b) using various aqueous solutions. The '*x*' refers to the applied initial Al concentration in solution ($[Al]_{initial}$), the 'b' to the base present in solution. (b) Amount of aluminum incorporated into the bulk of the silica material (Al_{ICP}) compared to the theoretical maximal amount of Al that is incorporated at the obtained mass yield (Al_{max}). (c) Al_{ICP}/Al_{max} as a function of $[Al]_{initial}$. The legend in (a) also applies in (b,c). (d) Bulk and surface Si/Al ratios (Si_{ICP}/Al_{ICP} and Si_{XPS}/Al_{XPS}, respectively) in S-*x*-NaOH samples.

Accepted Manuscript

This article is protected by copyright. All rights reserved.

10.1002/cctc.201701660

WILEY-VCH

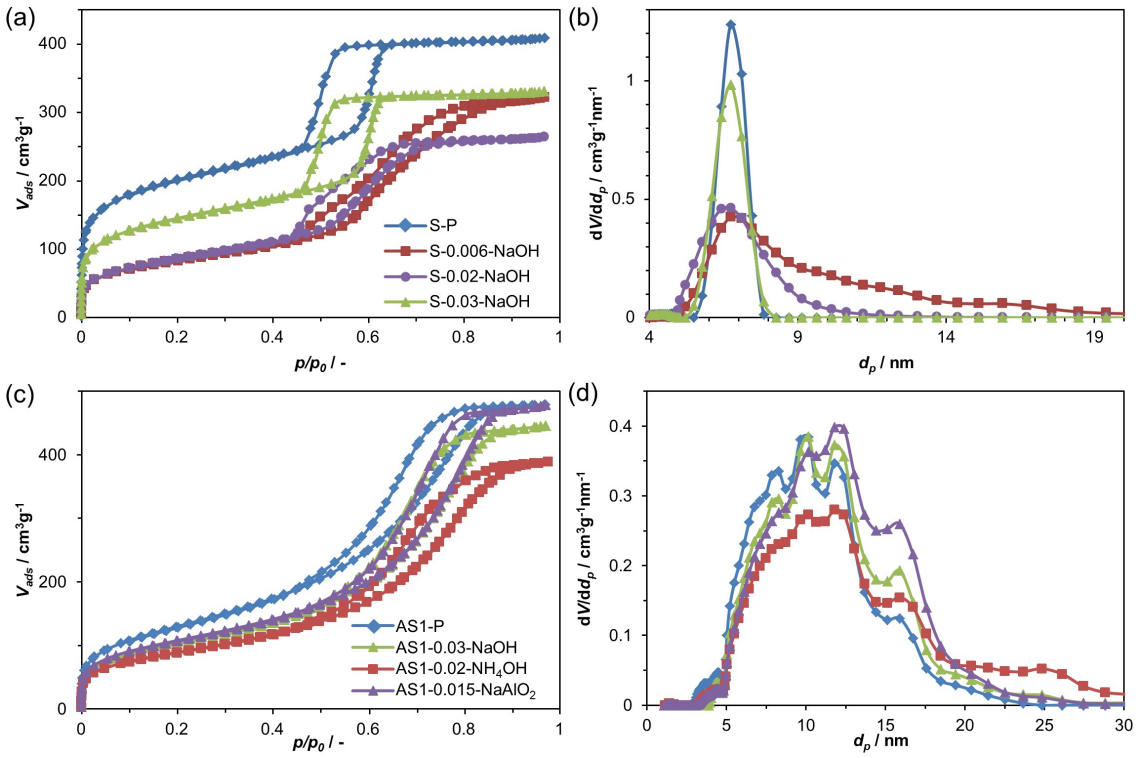

Figure 3. N_2 physisorption isotherms of (a) SBA-15 (S-*x*-NaOH) and (c) amorphous silica (AS1-*x*-b) samples before and after aluminations, and the accompanying adsorption NL-DFT PSDs (b, d, respectively). The '*x*' refers to the applied initial Al concentration in solution ($[Al]_{initial}$), the 'b' to the base present in solution.

Accepted Manuscript

This article is protected by copyright. All rights reserved.

10.1002/cctc.201701660

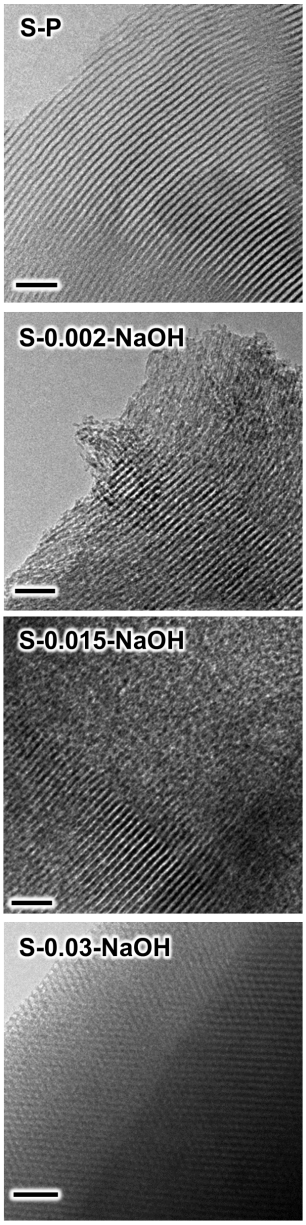

Figure 4. Bright-field TEM micrographs of selected SBA-15-derived samples. The scale bars are 50 nm.

Accepted Manuscript

This article is protected by copyright. All rights reserved.

10.1002/cctc.201701660

WILEY-VCH

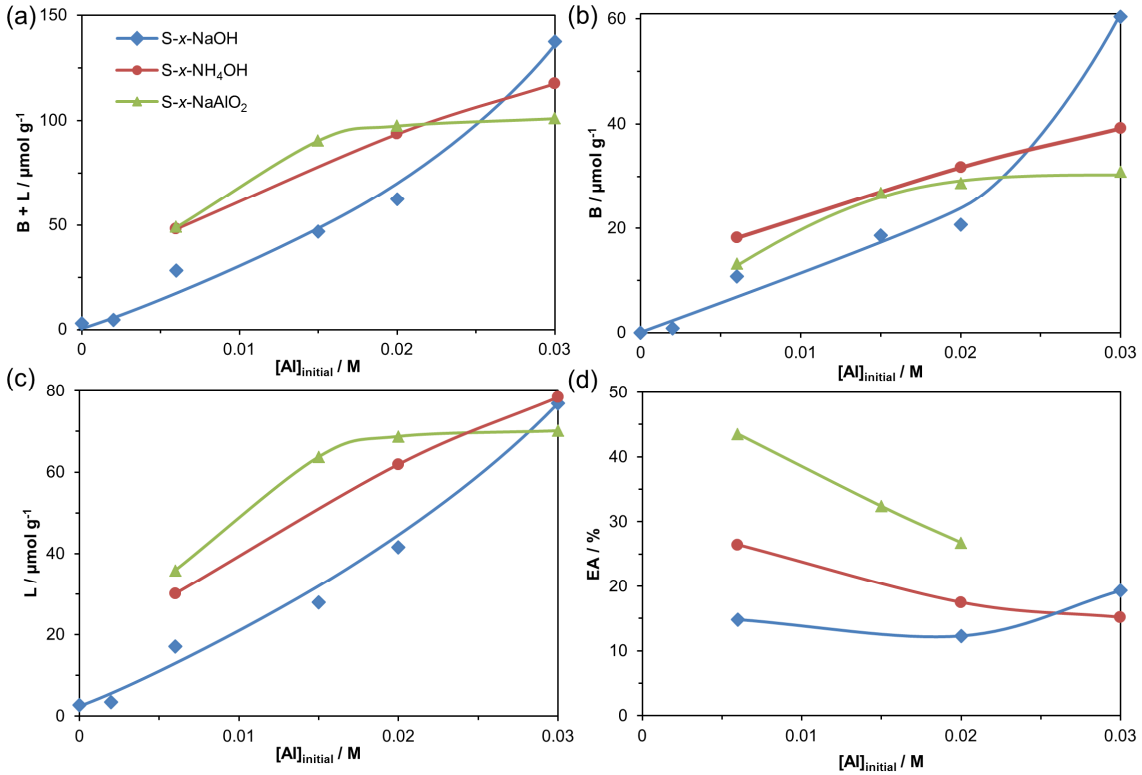

Figure 5. Number of acid sites in SBA-15 samples after aluminations as measured with pyridine probed FTIR. (b) Brønsted acid sites (B), (c) Lewis acid sites (L) and (a) the total acidity (B + L). (d) Effective acidity (EA) in SBA-15 samples after different alumination techniques: mol of acid sites per mol of Al in the solid (B + L / Al_{ICP}). The legend in (a) applies to the entire figure.

Accepted Manuscript

This article is protected by copyright. All rights reserved.

Table 2. Acidic properties of selected samples after different aluminations.

Sample	B[a] (µmol g^{-1})	L[a] (µmol g^{-1})	B/L (-)	B+L[a] (µmol g^{-1})	EA[b] (%)
S-0.03-NaOH	60	77	0.78	137	19
S-0.02-NH_4OH	32	62	0.52	94	18
S-0.03-NH_4OH	39	78	0.50	117	15
S-0.015-$NaAlO_2$	27	64	0.42	91	32
S-0.03-$NaAlO_2$	31	70	0.44	101	-
AS1-0.03-NaOH	15	46	0.33	61	9[g]
AS1-0.02-NH_4OH	21	46	0.46	67	13[g]
AS1-0.015-$NaAlO_2$	11	46	0.24	57	20[g]
ASA-6	42	78	0.54	120	5
ASA-0.4	16[d]	70[d]	0.23	86[d]	1
γ-Al_2O_3	0	103	-	103	~0
USY-40	79[e]	13[e]	6.1	92[e]	24
USY-2.6	180[f]	116[f]	1.55	296[f]	7

[a]Brønsted (B), Lewis (L) and total (B + L) acidity as measured with PP-FTIR. [b]Effective acidity (calculated as B + L / Al_{ICP}). [d]SIRAL 30 from ref. [9]. [e]From ref. [22]. [f]From ref. [26]. [g]The Al content was not measured, but calculated assuming the Al incorporation (91%) was the same as in the corresponding SBA-15 samples (following **Figure 2c**).

Accepted Manuscript

This article is protected by copyright. All rights reserved.

10.1002/cctc.201701660

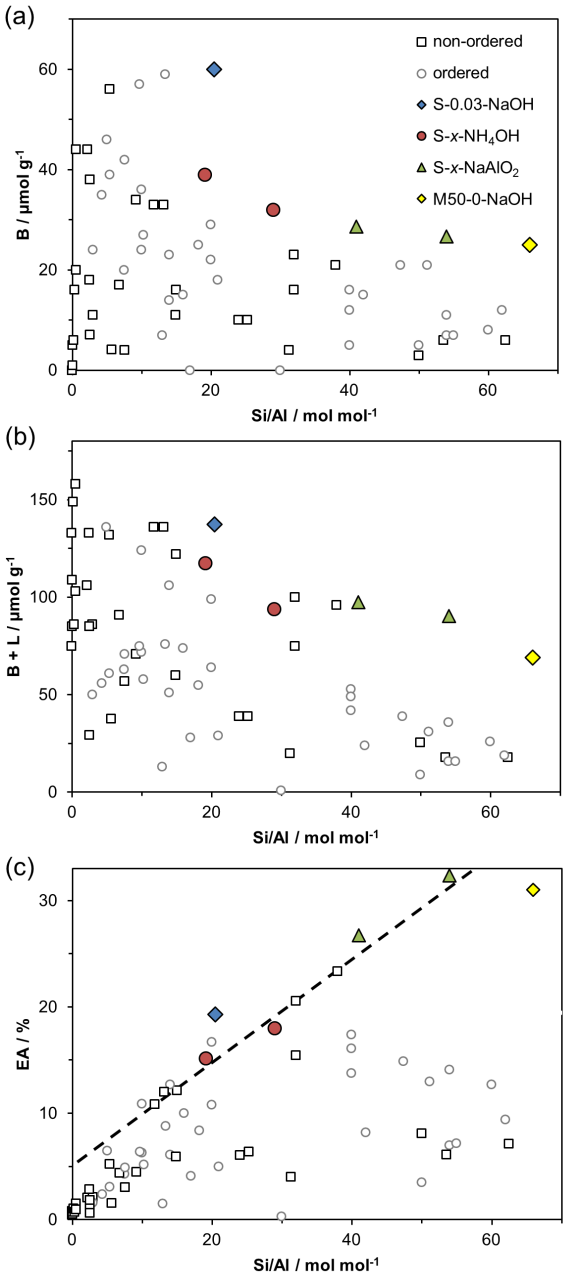

Figure 6. (a) Brønsted acidity (B), (b) Brønsted and Lewis acidity (B + L), and (c) effective acidities (EA, equal to (B + L)/Al_{ICP}), of ordered and non-ordered amorphous silica-aluminas as a function of the bulk Si/Al ratio. 'M50-0-NaOH' relates to an alkaline-activated Al-containing MCM-41 reported in ref. [20]. The dashed line in (c) highlights the samples which display the highest effective acidity as a function of the (bulk) Si/Al ratio.

Accepted Manuscript

This article is protected by copyright. All rights reserved.

10.1002/cctc.201701660

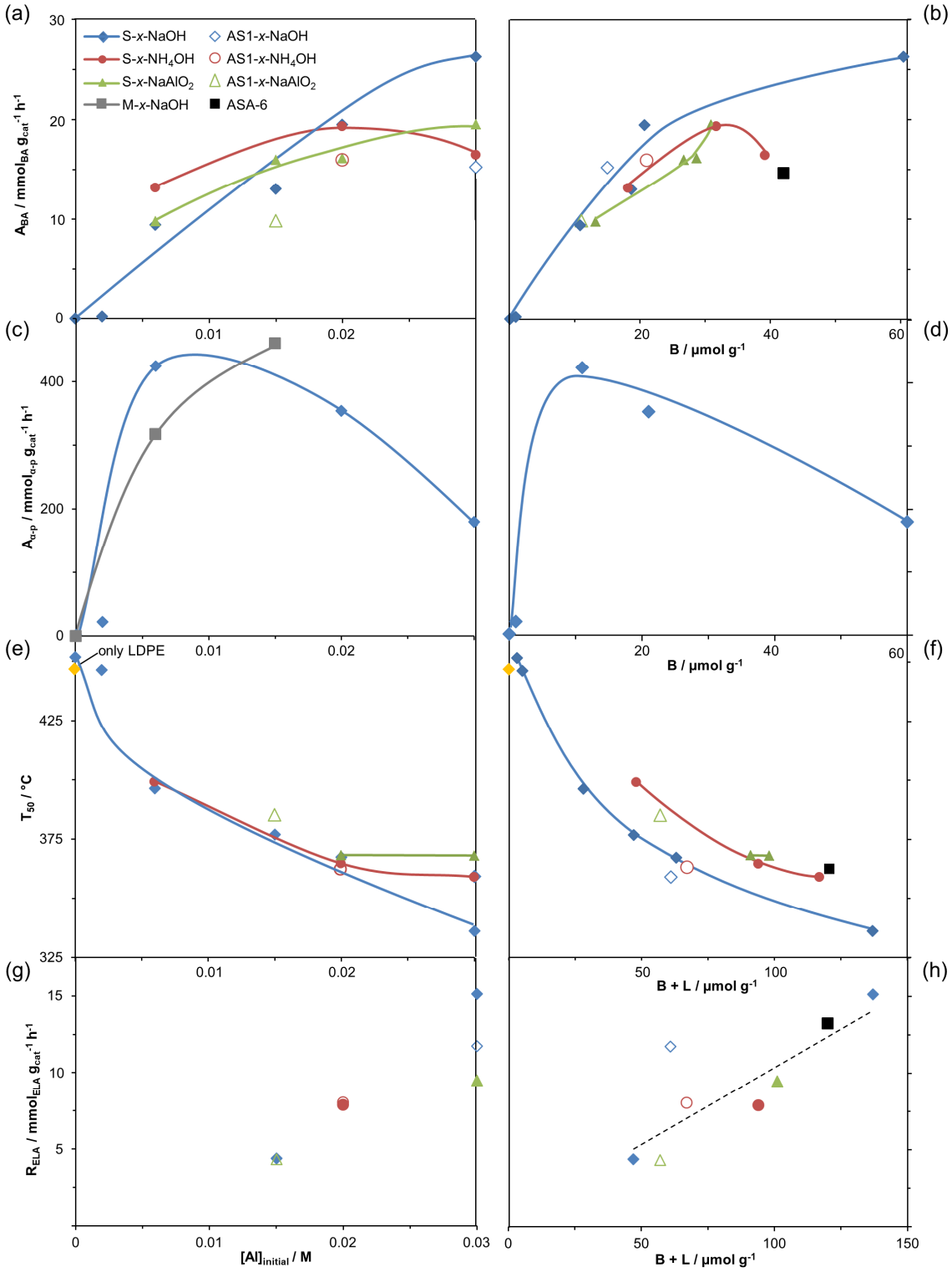

Figure 7. Catalytic performance of aluminated amorphous silicas as a function of initial Al concentration ($[Al]_{initial}$), the Brønsted acidity (B), and the total Brønsted and Lewis acidity (B + L). (a,b) Activity in the conversion of benzyl alcohol (A_{BA}), (c,d) activity in the conversion of α-pinene ($A_{\alpha\text{-}p}$), (e,f) temperature of 50% LDPE conversion to volatile products (T_{50}), and (g,h) the formation rate of ethyl lactate after 1 hour (R_{ELA}) in the conversion of 1,3-dihydroxyaceton. The legend in (a) applies to the entire figure.

This article is protected by copyright. All rights reserved.

Accepted Manuscript

WILEY-VCH

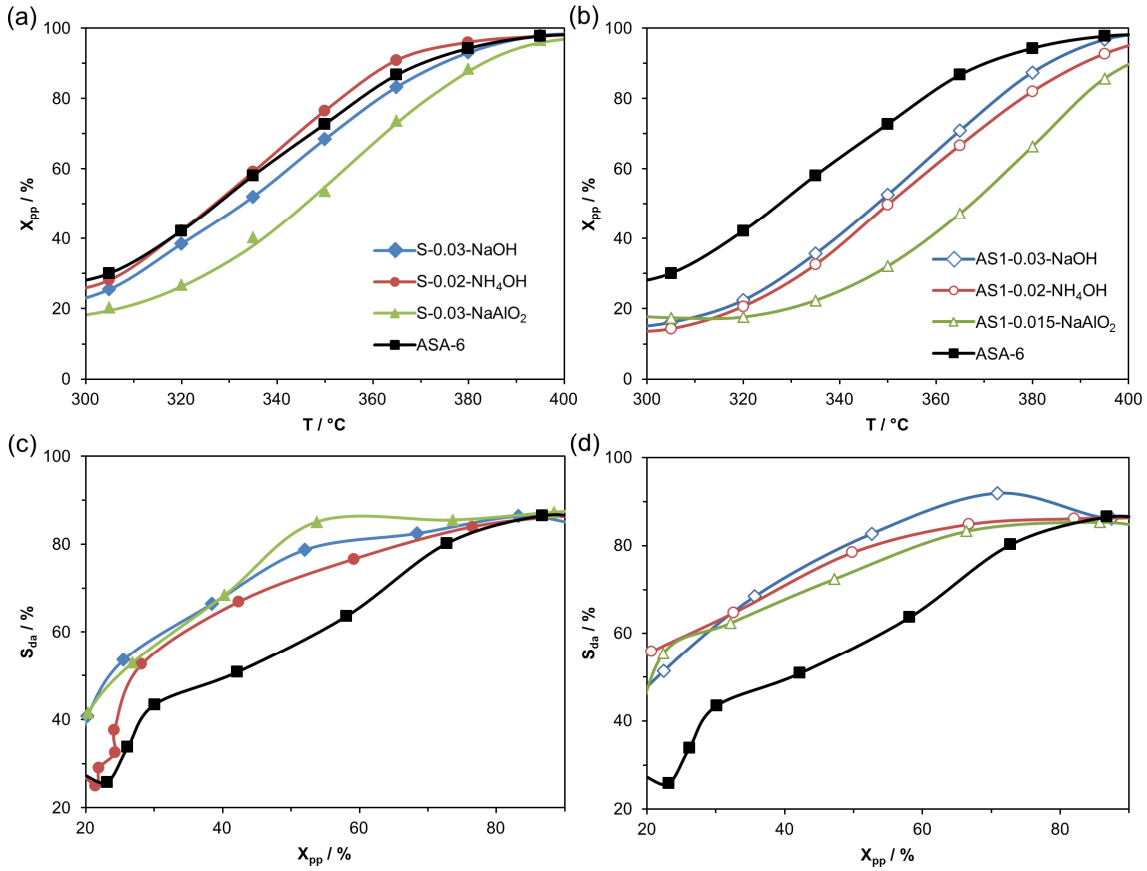

Figure 8. Conversion of propyl phenol (X_{pp}) for increasing temperatures using aluminated SBA-15 (a) or silica gel (b) as acid catalyst. Selectivity towards dealkylated products, phenol and propylene (S_{da}), versus the X_{pp} using aluminated SBA-15 (c) or silica gel (d) as acid catalyst. The legends in (a) and (b) respectively also apply in (c) and (d).

Accepted Manuscript

This article is protected by copyright. All rights reserved.

10.1002/cctc.201701660

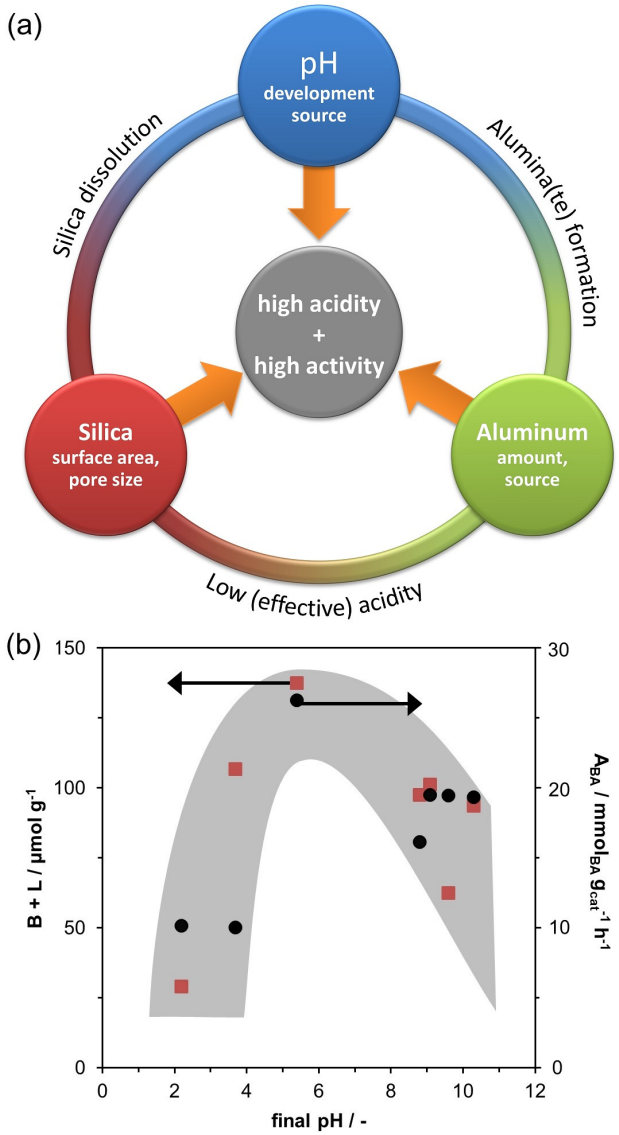

Figure 9. (a) The three main parameters required for the efficient creation of acid sites in amorphous silica. The potential detrimental effect of a suboptimal parameter is described in the outer circle between the two remaining parameters. (b) Total acidity (B + L) and activity in the conversion of benzyl alcohol (A_{BA}) as a function of the final pH in the alumination solution from S-*x*-b samples (pH values are listed in **Table S3**).

Accepted Manuscript

This article is protected by copyright. All rights reserved.

WILEY-VCH

The preparation of aluminosilicates by facile room-temperature post-synthesis alumination of silica is presented. Controlling the pH of Al-containing aqueous solutions yields porous aluminosilicates with superior acidity and stability. The effectivity of the method is demonstrated on several silica sources. Catalytic evaluation in five distinct acid-catalyzed reactions underline the potential of the developed materials.

Amorphous aluminosilicates

D. Verboekend,* B. Sels,*

Synthetic & Catalytic Potential of Amorphous Mesoporous Aluminosilicates Prepared by Post-Synthetic Aluminations in Aqueous Media

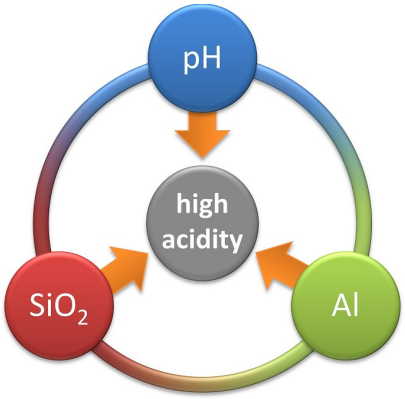

Accepted Manuscript

This article is protected by copyright. All rights reserved.